Manipulation of a Bose-Einstein condensate by a time-averaged orbiting potential using phase jumps of the rotating field

P. W. Cleary, T. W. Hijmans, and J. T. M. Walraven
Van der Waals–Zeeman Institute of the University of Amsterdam, Valckenierstraat 65, 1018 XE Amsterdam, The Netherlands
(Received 28 September 2010; published 30 December 2010)

We report on the manipulation of the center-of-mass motion ("sloshing") of a Bose-Einstein condensate in a time-averaged orbiting potential (TOP) trap. We start with a condensate at rest in the center of a static trapping potential. When suddenly replacing the static trap with a TOP trap centered about the same position, the condensate starts to slosh with an amplitude much larger than the TOP micromotion. We show, both theoretically and experimentally, that the direction of sloshing is related to the initial phase of the rotating magnetic field of the TOP. We show further that the sloshing can be quenched by applying a carefully timed and sized jump in the phase of the rotating field.

DOI: 10.1103/PhysRevA.82.063635 PACS number(s): 03.75.Kk, 37.10.Gh, 34.10.+x, 45.50.−j

I. INTRODUCTION

Time-averaged potentials (TAP) offer a versatile tool for trapping both charged and neutral particles. For neutral atoms the most common example in this class of traps is the time-averaged orbiting potential (TOP), which was used in the experiments in which the first Bose-Einstein condensate (BEC) was created [1,2]. The TOP trap consists a magnetic quadrupole trap [3,4] shifted by a uniform magnetic modulation field rotating at a high (audio) frequency. As this rotation is slow as compared with the Larmor precession of the atomic magnetic moments, the atoms remain polarized with respect to the instantaneous effective magnetic field [5] as follows from the adiabatic theorem. On the other hand, the rotation is fast as compared with the orbital motion of the atoms. As a consequence, the atomic motion consists of a fast rotating part (micromotion), superimposed on a slow oscillating part (macromotion). In the simplest theoretical description, the static approximation, the micromotion is eliminated by time averaging the instantaneous potential over a full cycle of the modulation field.

Suppose we load a particle with given momentum $\mathbf{p}_0$ at position $\mathbf{r}_0$ in a TOP trap using a sudden switch-on procedure. One might naively guess that the ensuing motion is given by the dynamics in the TAP, subject to the initial conditions $\mathbf{r} = \mathbf{r}_0$ and $\mathbf{p} = \mathbf{p}_0$, but this guess turns out to be wrong. In fact, one can show that the initial conditions for the slow motion depend on the phase of the TOP at the time of switch-on. This phenomenon was analyzed by Ridinger and coworkers [6,7] for the special case of a one-dimensional rapidly oscillating potential (ROP) with zero average. Ridinger *et al.* also showed, first for a classical particle [6] and subsequently for the quantum case [7], that the amplitude and energy associated with the slow motion can be altered by applying a suitable phase jump in the rapidly oscillating field.

In this paper we show, both theoretically and experimentally, that the dependence on the initial phase and the possibility of influencing the motion by phase jumps are also present for a two-dimensional rotating TOP field. In particular we show that a cloud of atoms that is initially at rest with zero momentum acquires a sloshing motion as soon as the TOP is suddenly switched on. This is true even if the cloud is initially at the minimum of the effective potential. The amplitude of this slow macromotion is much larger than that of the fast micromotion, while the direction of sloshing depends on the TOP phase at switch-on. We also demonstrate that this macromotion can be almost entirely quenched by applying a carefully timed and sized phase jump in the TOP field.

The motion of atoms and ultracold atomic clouds in TOP traps has been extensively described in the literature. Following the achievement of the first BEC [2], the use of the axially symmetric TOP was described theoretically in Refs. [8–13] and explored experimentally by other groups [14–19] to study properties of the BEC. The idea of the TOP was extended to an asymmetric triaxial TOP trap developed by Ref. [15] and used by other groups [17,18]. A number of other variations were introduced: In many cases, it turns out to be convenient to switch on the TOP after a preparative stage of cooling in a conventional static trap such as a magnetic quadrupole trap (see, e.g., Ref. [15]), an optically plugged magnetic quadrupole [20], and Ioffe-configurations [21–23]. Often the transfer of the cloud from the static to the TOP trap cannot be performed adiabatically for topological reasons. Bearing this in mind, it becomes relevant to carefully analyze the dynamics that may be induced by a sudden switch-on of the TOP. In addition, applications that require manipulation of a BEC are heavily dependent on precise control of the location of the atomic cloud and can thus benefit from the techniques described.

In our experiments the condensate is prepared in a Ioffe-Pritchard (IP) trap before transferring to a TOP. This procedure induces the "sloshing motion." Although our method is very specific, it is typical for any sudden change of a TOP geometry in amplitude and/or phase. In our case the transfer was chosen because the use of radio-frequency-induced evaporative cooling is more efficient in a static magnetic trap than in a TOP. Once transferred to the TOP we can create trapping geometries that are difficult to realize using a static magnetic potential without introducing Majorana losses associated with the presence of zero-field points. An example is the double-well potential used in Ref. [21].

The remainder of this paper is organized as follows. In Sec. II we calculate the motion of a cloud of atoms in a TOP that at switch-on is at rest at the center of the trap. We discuss the motion that results and derive the conditions under which

a phase jump can lead to a substantial reduction of the energy associated with the slow motion of the cloud. In Sec. III we discuss the experimental details and the preparation of the BEC and its transfer to the TOP. In Sec. IV we present the experimental results and compare them with the theory of Sec. II. Finally in Sec. V we give a summary and conclusion.

II. THEORY

A. Time-averaged Ioffe-Pritchard potential

In the literature the term TOP is most often used for a spherical-quadrupole trap combined with a rotating uniform magnetic modulation field. In this paper we will use TOP in a broader context, to include the magnetic trapping potential created by combining a IP trap with rotating modulation field. Challis *et al.* [13] have shown that the dynamical eigenstates of a degenerate Bose gas in a TOP are given by solutions of the usual Gross-Pitaevskii equation but taken in a circularly translating reference frame, that is, a reference frame the origin of which performs a rapid circular motion but retains a constant orientation. In particular this implies that the center of mass of a condensate in its ground state performs the same micromotion in a TOP as a point particle with the magnetic moment of an atom. In this spirit we use as a ^{87}Rb condensate to study the micromotion and macromotion in a TOP.

We consider a cigar-shaped IP potential [4,24,25]

$$U(\boldsymbol{\varrho},z) = \mu\sqrt{\alpha^2\varrho^2 + \left(B_0 + \tfrac{1}{2}\beta z^2\right)^2}, \tag{1}$$

where $\boldsymbol{\varrho}(t)$ is the radial position of a test atom with respect to the IP symmetry axis, μ the magnetic moment of the atom, and α, β, and B_0 the parameters for the radial gradient, axial curvature, and offset value of the IP magnetic field, respectively. Equation (1) represents an approximate expression for the IP trap that is valid for $\alpha^2 \gg \beta B_0$ and in the limit $\varrho \ll \alpha/\beta$ [4,24,25].

In the presence of the TOP field we transform to the circularly translating frame [13] and have

$$\boldsymbol{\varrho}(t) = \{x - \rho_m \cos(\omega t + \phi_m), \quad y - \rho_m \sin(\omega t + \phi_m)\}, \tag{2}$$

where $\{x,y,z\} \equiv \{\boldsymbol{\rho},z\} \equiv \mathbf{r}$ is the position of the atom in the laboratory frame and the IP symmetry axis is displaced over a distance $\rho_m = B_m/\alpha$ in the direction

$$\hat{\boldsymbol{\rho}}_m = \{\cos(\omega t + \phi_m), \sin(\omega t + \phi_m)\} \tag{3}$$

by the uniform modulation field

$$\mathbf{B}_m = B_m\{\cos(\omega t + \phi_m), -\sin(\omega t + \phi_m)\} \tag{4}$$

applied perpendicular to the z axis. The y axis is taken along the vertical direction, the xz plane being horizontal. The modulation field $\mathbf{B}_m$ rotates at angular frequency $-\omega$ (phase $-\phi_m$) around the horizontal z axis as illustrated in Fig. 1. Notice that the sense of rotation of the IP-field minimum is opposite to that of the $\mathbf{B}_m$ field, in contrast with the original TOP configuration [1], where the field zero rotates in the same direction as the bias field. This reflects the difference between the 2D-quadrupole symmetry of the IP trap and the axial symmetry of the spherical-quadrupole trap. The rotation of the modulation field $\mathbf{B}_m$ also gives rise to a fictitious field $\mathbf{B}_\omega$

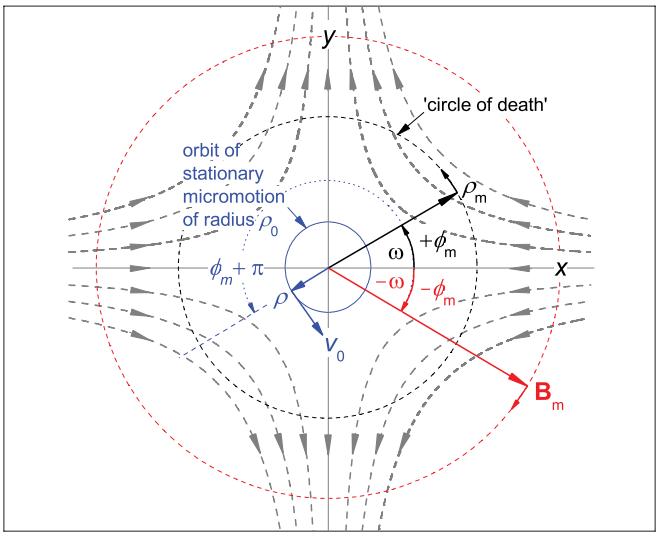

FIG. 1. (Color online) Schematic diagram of the magnetic field configuration in relation to the orbit of stationary micromotion (solid blue circle). The view is along the (horizontal) z axis. The orbital position and velocity of the micromotion are denoted by $\rho = -\rho_0\hat{\rho}_m$ and v_0, respectively. The IP symmetry axis rotates at frequency ω (with initial phase ϕ_m) around the z axis on the circle of radius ρ_m (dashed black circle). Note that the TOP field $\mathbf{B}_m = B_m\hat{\rho}_m$ rotates at frequency $-\omega$ (phase $-\phi_m$), reflecting the 2D-quadrupole symmetry (dashed red circle) of the IP trap.

that has to be added or subtracted from the offset field $\mathbf{B}_0$, depending on the sense of rotation,

$$\mathbf{B}_0 \to \mathbf{B}_0(1 \pm \mathbf{B}_\omega/\mathbf{B}_0) = \mathbf{B}_0(1 \pm \omega/\omega_L), \tag{5}$$

where $\omega_L = g_F\mu_B B_0/\hbar$ is the Larmor frequency of magnetic moment of the atoms, with g_F the hyperfine g factor and μ_B the Bohr magneton. In a standard TOP, the fictitious field in combination with a gradient of the quadrupole field gives rise to a shift of the equilibrium position of the cloud in the direction of the axis around which the field rotates [5,17]. In our IP TOP the axial field is homogeneous near the origin and the shift is absent; the change in B_0 turns out to be small and will be neglected in this paper.

For $\beta = 0$ and $B_0 = 0$ the potential $U(\boldsymbol{\varrho},z)$ corresponds to that of a two-dimensional quadrupole field with a zero-field line that rotates at distance ρ_m around the z axis as a result of the modulation. For $B_0 = 0$ the distance ρ_m is known as the radius of the "circle of death." For $B_0 < 0$ the potential corresponds to two TOP traps separated by $\Delta z = 2(2|B_0|/\beta)^{1/2}$ [21]. In this paper we will consider only the case $B_0 \geqslant 0$.

In the common description of the TOP one analyzes the motion in an effective potential, obtained by time averaging the static trap over a full rotation period of the $\mathbf{B}_m$ field. For Eq. (1) this procedure yields the effective potential

$$\mathcal{U}(\mathbf{r}) = \frac{1}{2\pi}\int_0^{2\pi} U(x - \rho_m\cos\zeta, y - \rho_m\sin\zeta, z)\,d\zeta, \tag{6}$$

where $\zeta = \omega t + \phi_m$. For the cigar-shaped IP potential we consider the condition

$$\omega \gg \Omega_\rho \gg \Omega_z, \tag{7}$$

where, for an atom of mass m, the quantity $\Omega_z = (\mu\ \beta/m)^{1/2}$ is the axial harmonic oscillation frequency in the effective potential $\mathcal{U}(0,0,z)$. Analogously, harmonic oscillation frequency in the radial plane is given by

$$\Omega_\rho = \sqrt{\frac{\mu\alpha^2}{m\bar{B}_0}\left(1-\frac{1}{2}B_m^2/\bar{B}_0^2\right)} \equiv \Omega, \tag{8}$$

where $\bar{B}_0 = (B_0^2 + B_m^2)^{1/2}$ is offset value of the effective potential at the origin [21].

The first inequality in Eq. (7) ensures that the fast and slow radial motions of the atoms can be separated, which is the well-known operating regime for a TOP trap [1]. The second inequality implies that the axial motion in the effective trap is slowest and that the motion can be treated as quasi two-dimensional in the radial plane.

To account for the acceleration due to gravity (g), the gravitational potential mgy has to be added to Eqs. (1) and (6). The main effect is to shift the minimum of the potentials in the negative y direction by the amount

$$\Delta y = g/\Omega^2. \tag{9}$$

This expression holds as long as the gravitational sag Δy is much smaller than the harmonic radius $\rho_h \equiv \bar{B}_0/\alpha$.

Since $\rho_h \geqslant \rho_m$, the effective potential (6) may be treated as harmonic as long as the motion is confined to a region around the z axis that is small compared with ρ_m. For our experiment the harmonic approximation holds rather well and is sufficient for gaining qualitative insight into the micro- and macromotion, as will be shown in Sec. II B. Refinements associated with switch-on transients and gravity are discussed in the Appendix. In the numerical analysis of Sec. II C, we solve the classical equations of motion in the full time-dependent potential Eq. (1). In this context we also comment on the validity of the harmonic approximation.

B. Micromotion and macromotion

To analyze the effect of switching on the $\mathbf{B}_m$ field at $t = 0$ we first consider an atom "at rest" in the center of the effective trapping potential $\mathcal{U}(\boldsymbol{\rho},z)$. Such an atom exhibits no period-averaged dynamics (no macromotion) but only circular micromotion at a frequency ω about the origin as illustrated in Fig. 1. The radius of this stationary micromotion,

$$\rho_0 = \frac{\mu\alpha}{m\omega^2}\left(1 + B_0^2/B_m^2\right)^{-1/2}, \tag{10}$$

follows from the condition $F_c = m\omega^2\rho_0$ for the centripetal force $\mathbf{F}_c = -\nabla_\rho U|_{\rho=0} = \mu\alpha(1 + B_0^2/B_m^2)^{-1/2}\hat{\boldsymbol{\rho}}_m$. The speed of this stationary micromotion,

$$v_0 = \omega\rho_0 = \frac{\mu\alpha}{m\omega}\left(1 + B_0^2/B_m^2\right)^{-1/2}, \tag{11}$$

is directed orthogonally to the direction $\hat{\boldsymbol{\rho}}_m$. Such pure micromotion results only if at $t = 0$ the atom is already moving at speed v_0 along a circle of radius ρ_0 around the origin and is located at position $\boldsymbol{\rho} = -\rho_0\hat{\boldsymbol{\rho}}_m$ (see Fig. 1). Obviously an atom at $t = 0$ at rest at the origin $\boldsymbol{\rho} = \{0,0\}$ does not satisfy these initial conditions, and as a consequence its macromotion will start with a finite launch speed. We will see that the result is elliptical motion at frequency Ω, with the long axis approximately perpendicular to the initial direction of $\hat{\boldsymbol{\rho}}_m$ and with a substantial amplitude of order $(\omega/\Omega)\rho_0$. Usually this motion is undesired, and our aim is to quantify it and subsequently quench it by imparting a phase jump to the TOP field.

It is worth mentioning that in the conditions relevant for the experiments described in this paper the amplitude and energy of the macromotion are not negligible compared with other relevant length and energy scales. The characteristic size of the condensate is given by the Thomas-Fermi radius, which turns out be slightly smaller than the macromotion amplitude. Likewise, the energy associated with the macromotion is at least as large as the chemical potential.

To gain insight into the way in which the sudden switch-on of the TOP influences the macromotion of an atom initially at rest at the origin, we first consider a simple model in which it is assumed that the motion in the radial plane can be decomposed into two harmonic components, oscillating at the micromotion and macromotion frequencies ω and Ω, respectively. The position $\boldsymbol{\rho}(t)$ and velocity $\dot{\boldsymbol{\rho}}(t)$ are given by

$$\begin{aligned}\boldsymbol{\rho}(t) &= \{\rho_0\cos(\omega t+\phi), \rho_0\sin(\omega t+\phi)\}\\ &\quad + \{X_0\cos(\Omega t+\varphi_x),\ Y_0\sin(\Omega t+\varphi_y)\},\end{aligned} \tag{12}$$

$$\begin{aligned}\dot{\boldsymbol{\rho}}(t) &= \{-v_0\sin(\omega t+\phi), v_0\cos(\omega t+\phi)\}\\ &\quad + \{-V_{0,x}\sin(\Omega t+\varphi_x),\ V_{0,y}\cos(\Omega t+\varphi_y)\},\end{aligned} \tag{13}$$

where X_0 (Y_0) is the amplitude, $V_{0,x} = \Omega X_0$ ($V_{0,y} = \Omega Y_0$) the velocity amplitude, and φ_x (φ_y) the initial phase of the macromotion in the x (y) direction; ϕ is the initial phase of the micromotion. The atom starts at rest at the origin; hence the initial conditions are $\boldsymbol{\rho},\dot{\boldsymbol{\rho}} = 0$ at $t = 0$. If the condition

$$\omega \gg \Omega \tag{14}$$

is satisfied, the acceleration due to the micromotion dominates over that of the macromotion. The total acceleration may be approximated by $\ddot{\boldsymbol{\rho}} \simeq \mathbf{F}_c/m$. In other words, $\ddot{\boldsymbol{\rho}}$ points in the direction $\hat{\boldsymbol{\rho}}_m$, which is opposite to the direction of $\boldsymbol{\rho}$ (see Fig. 1). Hence, the initial phase of the micromotion is $\phi \simeq \phi_m + \pi$, where ϕ_m is fixed by the phase of the rotating $\mathbf{B}_m$ field [26]. Without loss of generality we can set $\phi_m = 0$, which means that $\hat{\boldsymbol{\rho}}_m$ is oriented along the positive x direction at $t = 0$. With this choice and setting $\phi = \phi_m + \pi$, we find from the initial conditions $\varphi_x,\varphi_y = 0$, $X_0 = \rho_0$, and $Y_0 = (\omega/\Omega)\rho_0$. Substituting these values in Eq. (12) we obtain an equation for the macromotion representing an elliptical orbit with its major axis oriented perpendicular to the instantaneous direction $\hat{\boldsymbol{\rho}}_m$ of the $\mathbf{B}_m$ field at $t = 0$. Since the amplitude of the macromotion along its major axis is larger than the micromotion by the factor ω/Ω, a substantial sloshing motion results from the sudden switch-on. Note that with increasing ω, the micromotion amplitude ρ_0 decreases like $1/\omega^2$, whereas the amplitude of the sloshing motion Y_0 decreases only like $1/\omega$. For this reason the sloshing cannot be neglected in most practical cases involving audio-frequency modulation.

C. Numerical analysis

To validate the analytical model introduced in Sec. II B, we numerically integrate the classical equations of motion in the

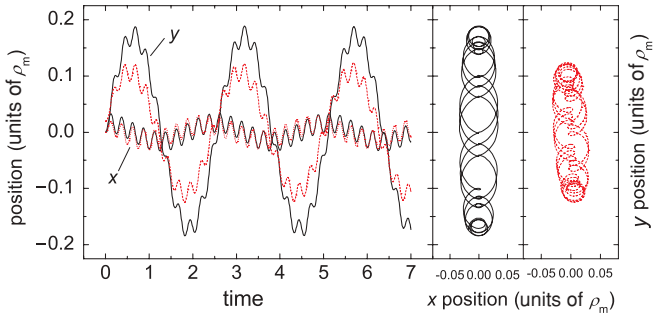

FIG. 2. (Color online) Numerically calculated trajectories in the xy plane with the x and y positions shown against time (left) and parametric plots of the same trajectory in the xy plane (middle and right) of a particle initially at rest at the origin, after instant switch-on (black lines). The dotted red curves correspond to a switch-on time of 3 μs of the TOP field, a settling time for the value of B_0, as well as the presence of gravity. The trap frequencies are $\omega/2\pi = 4$ kHz and $\Omega/2\pi = 394$ Hz. Units are scaled to the TOP radius ρ_m.

full time-dependent potential given by Eq. (1) for $z = 0$, $v_z = 0$, and $\phi_m = 0$. The result for the trajectory is given in Fig. 2 and exhibits the sloshing macromotion already described. The choice of parameters is such that it matches the experimental conditions that will be presented in Sec. III.

The drawn black lines in Fig. 2 correspond to a sudden switch-on of the TOP trap at $t = 0$ for an atom initially at rest at the origin in the absence of gravity. The figure clearly shows the micromotion superimposed onto the macromotion orientated along the y direction. The amplitudes and phases of the macromotion obtained by fitting Eq. (12) to the results of the numerical calculation agree accurately with the analytical model of Sec. II B (see Table I). A more detailed comparison reveals that anharmonicities play a minor role; the harmonics of both the micro- and macromotion have amplitudes that are at least two orders of magnitude smaller than those of the fundamentals.

In order to allow a better comparison with the experiments to be discussed, we have also performed the numerical analysis including several refinements that pertain to our specific experimental situation. These effects are: (a) a difference (δy) in gravitational sag between the IP and the TOP trap, (b) an exponential switching transient of the current in the TOP coils and correspondingly in the $\mathbf{B}_m$ field ($\tau_{1/e} = 3$ μs), and (c) a switching transient of $\sim$0.5 ms in the offset field from $B_0 = 9.5 \times 10^{-5}$ T at $t = 0$ to the final value $B_0 = 3.1 \times 10^{-5}$ T.

TABLE I. Comparison of numerical results (num) with the analytical model (AM); +ab: including refinements (a) and (b); +abc: all refinements included.

	ϕ_m	θ/π	φ_x/π	φ_y/π	X_0/ρ_0	Y_0/ρ_0
num	0	0	0	0	1	10.2
AM	0	0	0	0	1	10.2
num+ab	0	0.024	0.22	0.04	1.34	10.2
AM+ab	0	0.024	0.23	0.04	1.34	10.2
num+abc	0	0.017	0.20	0.06	0.82	6.5
AM+abc	0	0.021	0.23	0.06	0.85	6.5

The initial gravitational sag in the IP trap is 1.2 μm. When switching on the TOP, the sag Δy jumps in $\sim$3 μs to 1.7 μm and settles in $\sim$0.5 ms to its final value 1.6 μm due to the decrease of B_0. Thus the gravitational sag increases jumpwise and settles at $\delta y = 0.4$ μm. During the same transient the radius of the stationary micromotion grows from $\rho_0 = 0.21$ μm to $\rho_0 = 0.33$ μm, and Ω increases by about 5%.

The dotted red traces in Fig. 2 correspond to the numerical calculation, including all the already mentioned refinements relevant to the experiments. We have also investigated the effects of gravity, $\mathbf{B}_m$ switching, and B_0 switching separately. We find that the main effect of the settling time of B_0 is to reduce the amplitude along the major axis by $\sim$35%. The combined effect of changing gravitational sag and $\mathbf{B}_m$ transient is to slightly increase the x amplitude as well as to produce a slight tilt angle of the trajectory (see rightmost panel of Fig. 2).

The tilt angle θ of the macromotion also follows from a fit of Eq. (12) to the numerical results. For known values of X_0, Y_0, φ_x, and φ_y the angle of rotation ϑ to align the coordinate system along the major and minor axis is given by

$$\vartheta = \tfrac{1}{2}\tan^{-1}\left[2\sin(\varphi_x - \varphi_y)X_0Y_0\big/\left(Y_0^2 - X_0^2\right)\right]. \quad (15)$$

For $\phi_m = 0$ the tilt angle equals the rotation angle ($\theta = \vartheta$).

The results of a fit of Eq. (12) to the numerical results including only the refinements (a) and (b), as well as a fit including all three refinements (a), (b), and (c) are also given in Table I. Extending the analytical model to include the refinements (a) and (b) is straightforward and given in detail in the Appendix. The expressions for the amplitudes and phases depend on the model parameter τ_0 and are given by Eqs. (A6)–(A9) in the Appendix. The model parameter τ_0 is chosen by ensuring that the value of the tilt angle θ of the model reproduces that of a fit to the numerical solution for zero settling time, $\theta = 0.024\pi$. This results in $\tau_0 = 3.5$ μs. Excellent agreement is obtained with the numerical model as is shown in Table I. Insight in the cause of the reduction of the major-axis amplitude associated with the settling behavior of B_0 can also be gained using the analytical model. As discussed in the Appendix the major refinement is to change the launch speed corresponding to the initially smaller value of ρ_0. Although this refinement captures the origin of the 35% reduction of the major-axis amplitude, Table I shows that the overall agreement with the numerical model is less favorable.

D. Phase jumps

Let us now analyze how the macromotion can be quenched. For a one-dimensional ROP it was demonstrated in Ref. [6] that the amplitude of the macromotion can be quenched by an appropriate phase jump of the modulation field. For the 2D motion in a TOP, the success of such an approach is not *a priori* obvious because the phase jumps for the x and y motion cannot be selected independently. Yet, as will be shown, for the TOP as well it is possible to quench both the X_0 and Y_0 amplitudes more or less completely by imposing a single phase jump $\Delta\phi_m$ to the $\mathbf{B}_m$ field.

For clarity we first restrict ourselves to the case $\phi_m = 0$ and neglect the effects of gravity and switching transients. This means that the cloud is launched at $t = 0$ in the vertical y direction with a speed that is equal to v_0, the micromotion

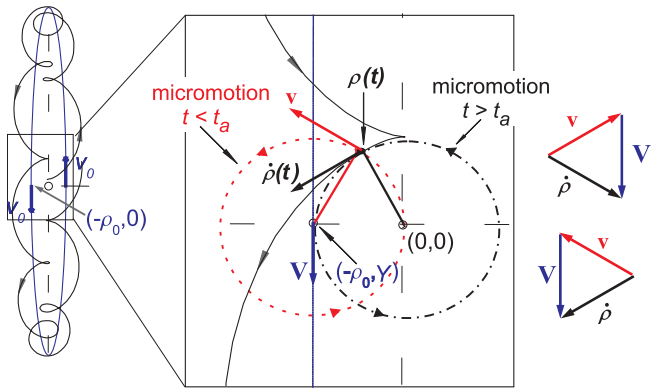

FIG. 3. (Color online) Explanatory diagram for the phase jump. Left: Cloud trajectory (black solid line) along with macromotion trajectory (blue dotted line). The black dashed lines are the symmetry axes of the trap, and the blue arrows show the macromotion velocity on crossing the x axis. Middle: Expanded view of boxed region of the left panel; $\rho(t)$ is the position of the cloud at the time of the phase jump. The red dashed (black dot-dashed) circle is micromotion just before (after) the phase jump at $t = t_a$. Right: Micromotion ($\mathbf{v}$) and macromotion ($\mathbf{V}$) velocity vectors add up to the total velocity vector $\dot{\rho}(t)$.

speed. As can be seen from the trajectory depicted on the leftmost side of Fig. 3, the macromotion speed will again be equal to v_0 when the cloud returns close to the origin after an integer number of macromotion half periods. The total velocity $\dot{\boldsymbol{\rho}}(t)$ is the vector sum of the micro- and macromotion velocities, and this quantity varies rapidly on a time scale of the micromotion period.

The essence of the quenching procedure is to apply the phase jump at a time t_a chosen in the interval $t_n - \Delta t < t < t_n + \Delta t$ around times $t_n = n(\pi/\Omega)$ corresponding to a multiple of the macromotion half period. We choose t_a such that $\dot{\boldsymbol{\rho}}(t_a)$ has a magnitude equal to v_0. When the cloud returns at the x axis the micro- and macromotion speeds are both v_0, and hence the resultant total velocity can be equal to v_0 only if the angle between the macro- and micromotion directions is either $2\pi/3$ or $-2\pi/3$ corresponding to two distinct micromotion phases $\phi_a \equiv \phi(t_a) = \omega t_{2n-1} + \phi = \pm\pi/3$ (see rightmost side of Fig. 3). In other words the micro- and macromotion velocity vectors form an equilateral triangle. For each of these cases a corresponding phase jump exists, $\Delta\phi_m = \pm\pi/3$, respectively, such that $\hat{\boldsymbol{\rho}}_m$ is set perpendicular to $\dot{\boldsymbol{\rho}}(t_a)$, which sets the macromotion velocity to zero. The result is pure micromotion if the orbit into which the particle is kicked is centered around the origin. For each of the two choices of ϕ_a, pure micromotion results only if the macromotion position at the time of the phase jump is equal to $(\pm\rho_0,0)$, where the $\pm$ sign applies for even (odd) n. Complete quenching can be achieved only for specific choices of the ratio ω/Ω. The change of orbit upon a phase jump is explained pictorially in the center panel of Fig. 3.

We now generalize to the case where the ratio ω/Ω is not precisely fine tuned and allow for the possibility that the macromotion speed deviates slightly from the value v_0 that we have assumed. One can show that, also in this case, the maximal reduction in marcromotion energy resulting from a phase jump is achieved when the jump is applied at a time t_a when $\dot{\boldsymbol{\rho}}(t_a)$ has a magnitude equal to v_0. The value of $\Delta\phi_m$ is again selected such as to set $\hat{\boldsymbol{\rho}}_m$ perpendicular to $\dot{\boldsymbol{\rho}}(t_a)$. By reasoning similar to the case already described, we find that the condition of an equilateral triangle of the three velocity vectors is now replaced by one that is an isosceles-triangle condition with the micromotion velocity and $\dot{\boldsymbol{\rho}}(t_a)$ both having a magnitude v_0. This in turn means that the magnitude of the phase jump will deviate slightly from the values $\pm\pi/3$ already found. Also, the nearest distance to the x axis at which the isosceles-triangle condition can be met is in general not equal to zero. This means that some residual macromotion will be present after the phase jump, with an amplitude given by the distance to the origin of the center of the circular orbit into which the cloud is transferred by the phase jump. One can show that there is always a choice possible where the isosceles-triangle condition is satisfied such that this distance is approximately $2\rho_0$ or less. As a consequence, even in the worst case, the macromotion amplitude is reduced from $(\omega/\Omega)\rho_0$ to an amplitude of order ρ_0.

The criterion that the acceleration be set perpendicular to the total velocity at the time that the macromotion speed is equal to v_0 can be expressed by the following equation:

$$\Delta\phi_m = \arctan\left[\frac{\dot{\rho}_y(t_a)}{\dot{\rho}_x(t_a)}\right] - \phi(t_a) + (-1)^k\frac{\pi}{2}, \qquad (16)$$

where $\dot{\rho}_x(t_a) = -v_0\sin\phi(t_a) - V_{0,x}\sin(\Omega t_a + \varphi_x)$ and $\dot{\rho}_y(t_a) = v_0\cos\phi(t_a) + V_{0,y}\cos(\Omega t_a + \varphi_y)$ are x and y components of $\dot{\boldsymbol{\rho}}$ at time t_a and $k = 1$ for $\dot{\rho}_x(t_a) > 0$ and $k = 0$ for $\dot{\rho}_x(t_a) < 0$. We return to selection of the jump time and the use of Eq. (16) when discussing the measurement procedure in Sec. III B.

Examples of the numerical calculations of the quenching procedure are shown in Fig. 4. The near complete quenching of the macromotion shown in Fig. 4(a) is obtained for $\delta y = 0$ and $\tau = 0$ with phase jump $\Delta\phi_m = -\pi/3$ at time $t_a = 3.834$ ms in the time interval around $t_3 = 3\pi/\Omega$. In Fig. 4(b) the refinements (a), (b), and (c) are included in the simulation of the experiment. In this case the phase jump had to be adjusted to $\Delta\phi_m = -0.22\pi$ for maximum quenching. Note that the quenching is less complete. By adjusting, at constant Ω, the micromotion frequency to $\omega = 4.068$ kHz and the jump time to $t_a = 3.769$ ms, complete quenching similar to that shown in Fig. 4(a) was also obtained when including all refinements in the numerical model.

III. EXPERIMENTAL

A. Apparatus

The experiments are done with the apparatus described in detail in Refs. [27] and [28]. We produce a BEC of 2.5×10^5 atoms of ^{87}Rb in the $|F = 2, m_F = 2\rangle$ state in an IP trap using radio-frequency evaporative cooling. The symmetry axis (z axis) of the trap lies horizontal with trap frequencies ($\Omega_\rho/2\pi = 455(5)$ Hz, $\Omega_z/2\pi = 21$ Hz) and the magnetic-field offset $B_0 = 9.5(3) \times 10^{-5}$ T, $\alpha = 3.53$ T/m, and $\beta = 266$ T/m^2. The Thomas-Fermi radius of the BEC is 2.2 μm. The TOP field is produced by two pairs of coils, one in the x direction, the other in the y direction, as described

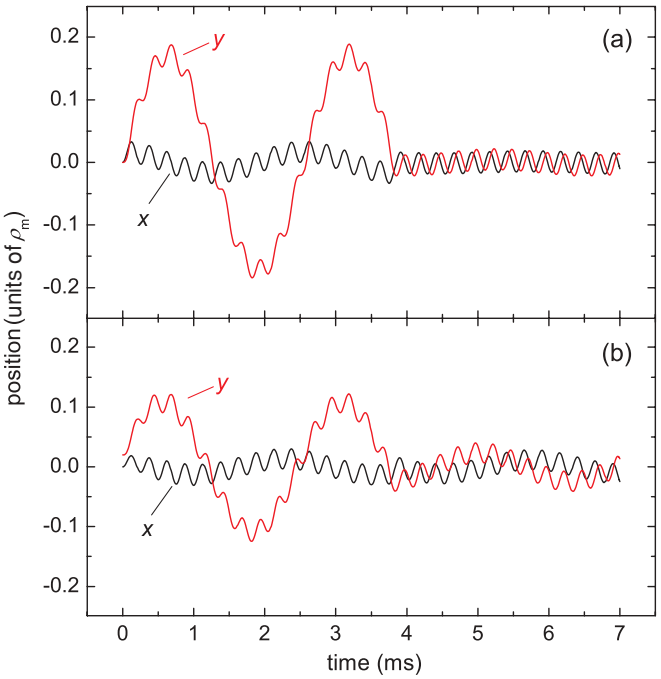

FIG. 4. (Color online) Numerically calculated radial trajectories in the x and y directions for the same trap parameters as used for Fig. 2, with a quenching phase jump $\Delta\phi_m$ applied at optimized $t = t_a \simeq t_3$ (three macromotion half periods). (a) Instant switching, no gravity: $\Delta\phi_m = -\pi/3$, $t_a = 3.834$ ms; (b) including switching transients and gravity: $\Delta\phi_m = -0.22\pi$, $t_a = 3.834$ ms.

previously in Ref. [21]. The coils consist of only two windings to keep the inductance low. The current for the TOP is generated by a TTI 4 channel arbitrary waveform generator (TGH 1244), amplified by a standard audio amplifier (Yamaha AX-496). The current used is $I_m = 3.0$ A, and the field produced is $B_m = 6.8(2) \times 10^{-5}$ T. All measurements in the TOP are done with $\Omega/2\pi = 394(4)$ Hz ($B_0 = 3.1 \times 10^{-5}$ T). Detection is done by time-of-flight absorption imaging along the z axis using a one-to-one transfer telescope to image the xy plane onto a Princeton TE/CCD-512EFT CCD camera with 15 μm pixel resolution. All measurements are carried out with the same flight time $\Delta t_{\mathrm{TOF}} = 23$ ms, giving rise to an expanded cloud radius of $\sim$140 μm.

B. Measurement procedure

Our experiments on phase-jump-controlled motion in a TOP trap are done with the $\mathbf{B}_m$ field operated at $\omega/2\pi = 4$ kHz. This frequency is sufficiently high ($\omega/\Omega \gtrsim 10$) to satisfy the "TOP condition" [Eq. (14)]. The frequency is chosen lower than in a typical TOP to ensure that the speed of the stationary micromotion, 9 mm/s as estimated with Eq. (11), is accurately measurable. In the experiments we start with an equilibrium BEC in the IP trap already described. At $t = 0$ we switch on the $\mathbf{B}_m$ field, using B_0 to tune the measured trap frequency to $\Omega/2\pi = 394$ Hz. As the trap minimum shifts down by $\delta y = 0.40$ μm, the initial position of the cloud is slightly above the trap center. The $1/e$-switching time of the $\mathbf{B}_m$ field was measured to be $\tau \approx 3$ μs, which corresponds to $\omega\tau \approx 0.08$. When changed, the B_0 field settles to a new value after a damped oscillation with a frequency of 650 Hz and a damping time τ' of 0.56 ms. This corresponds to $\Omega\tau' \approx 0.2$. The velocity $\dot{\boldsymbol{\rho}}$ of the BEC in the radial plane at the time of release is determined by time-of-flight absorption imaging along the z axis. For the chosen flight time of 23 ms, a speed of 1 mm/s corresponds to a displacement of 23 μm with respect to a cloud released from the same position at zero velocity. A cloud released at rest at time t_{rel} is imaged at position $\mathbf{R}_0 = \boldsymbol{\rho}(t_{\mathrm{rel}}) + \frac{1}{2}\ddot{\boldsymbol{\rho}}_g \Delta t_{\mathrm{TOF}}^2$, where $\ddot{\boldsymbol{\rho}}_g$ is the gravitational acceleration. For a finite release velocity $\dot{\boldsymbol{\rho}}(t_{\mathrm{rel}})$ the cloud will be imaged at $\mathbf{R} = \dot{\boldsymbol{\rho}}(t_{\mathrm{rel}})\Delta t_{\mathrm{TOF}} + \mathbf{R}_0$.

In practice we may neglect the small variation in the release position due to the macromotion, approximating $\boldsymbol{\rho}(t_{\mathrm{rel}}) \simeq \rho(0)$, because this variation is smaller than the shot-to-shot reproducibility of the cloud position. From the model analysis of Sec. II B the variation in release position due to the macromotion is estimated to be $\delta\boldsymbol{\rho}(t_{\mathrm{rel}}) \lesssim (\omega/\Omega)\rho_0 \approx 4$ μm. The centroid of the image of the expanded cloud is determined using a simple Gaussian fitting procedure and has a shot-to-shot reproducibility of $\sim$8 μm, small as compared with the 140 μm radius of the expanded cloud. No improvement in shot-to-shot reproducibility was found by changing to a higher magnification. Since our measurements depend only on the position of the cloud center, they are insensitive to fluctuations in atom number or density. To reconstruct the motion of the condensate in the trap we image the cloud at $t = t_i$, where t_i is the holding time in the TOP. We obtain the release velocity by measuring the x and y components of the cloud centroid (R_x, R_y). A typical set of data is shown in Fig. 5. The micromotion is recognized as the rapid modulation on the slow macromotion. As the frequency of the micromotion is accurately known, we avoid aliasing by sampling the motion in steps of 0.025 ms, much shorter than the micromotion period. If we wish to look only at the macromotion in a stroboscopic manner, we can sample precisely at the micromotion period of 0.25 ms, with the best results obtained when sampling on the

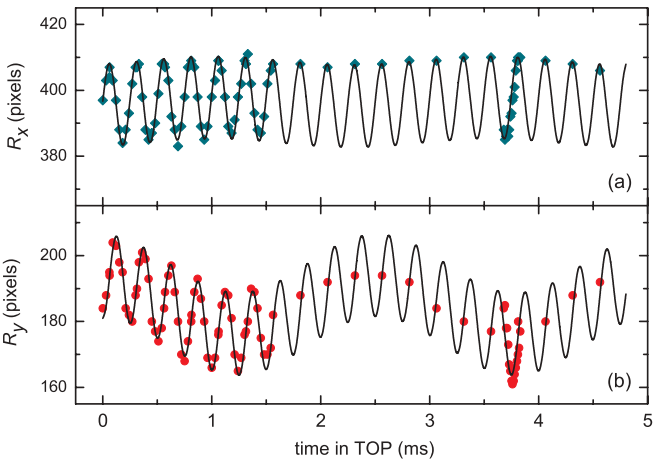

FIG. 5. (Color online) The centroid position after 23 ms TOF plotted in camera pixel units against holding time in the TOP trap. Upper datatset: R_x; lower dataset: R_y. The solid lines represent the fit of Eqs. (17) and (18) to the data. Note that by a stroboscopic measurement at 0.25 ms intervals the micromotion is eliminated. Each point represents a single measurement.

crests of the micromotion. Fitting the expressions

$$R_x = -v_0 \Delta t_{\mathrm{TOF}} \sin(\omega t + \phi) - V_{0,x} \Delta t_{\mathrm{TOF}} \sin(\Omega t + \varphi_x) + R_{0,x}, \quad (17)$$

$$R_y = v_0 \Delta t_{\mathrm{TOF}} \cos(\omega t + \phi) + V_{0,y} \Delta t_{\mathrm{TOF}} \cos(\Omega t + \varphi_y) + R_{0,y} \quad (18)$$

to the data and using the TOP frequency ω and Δt_{TOF} as known parameters, we obtain the amplitudes $v_0, V_{0,x}, V_{0,y}$ as well as the macromotion frequency Ω and the phases $\phi, \varphi_x, \varphi_y$. Note that the fit also yields the reference position $\mathbf{R}_0 = \{R_{0,x}, R_{0,y}\}$, but this information is superfluous for the reconstruction of the in-trap motion. Once these quantities are determined, the motion of the condensate in the TOP trap is readily reconstructed with Eq. (12).

To investigate the effect of phase jumps, we implement the approach described in Sec. II D. First we determine for given ω and Δt_{TOF} all parameters to reconstruct the motion with the method just described. This enables us to determine the time intervals $t_n - \Delta t < t < t_n + \Delta t$, where the cloud returns close to the origin, and choose within this interval the time t_a, where the total velocity $\dot{\boldsymbol{\rho}}(t_a)$ has magnitude v_0 as shown in Fig. 6(a). The red dashed lines correspond to the analytical model of Sec. II D for the case of instant switching: no gravity [the case of Fig. 4(a)]. The black solid lines correspond to the calculation including all relevant experimental constraints. The phase jump $\Delta\phi_m$ that sets $\hat{\boldsymbol{\rho}}_m$ perpendicular to $\dot{\boldsymbol{\rho}}(t_a)$ is given by Eq. (16). This optimal phase jump $\Delta\phi_m$ is plotted versus t_a in a time interval around $t_3 = 3\pi/\Omega$ in Fig. 6(b). For the case of instant switching, no gravity, the optimum phase jump is seen to be $\Delta\phi_m = -\pi/3$. At the chosen time t_a we vary the phase jump $\Delta\phi_m$ around the value suggested by Eq. (16) in search for optimal quenching. To reconstruct the residual

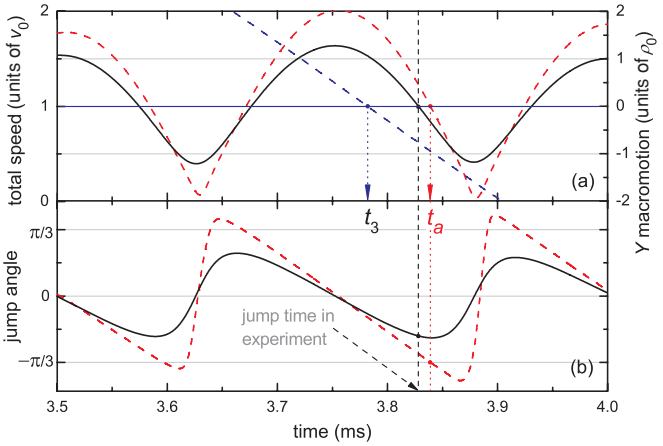

FIG. 6. (Color online) Illustration of how to choose the optimal phase jump and its timing. Both panels: solid black curve: experimental conditions; dashed red curve: analytical model of Sec. II D for the case of instant switching: no gravity. (a) Total speed of the cloud in units of the micromotion speed v_0 [optimal phase jump time t_a corresponds to $\dot{\rho}(t_a) = v_0$]; the dashed blue line (scale on right) shows the Y component of the macromotion position crossing zero at $t = t_3$ (stationary micromotion can be achieved by adjusting ω such that $t_3 = t_a$). (b) Optimal phase jump as a function of jump time as calculated by Eq. (16).

macromotion, we hold the cloud for a variable additional time t_b, before TOF imaging at time $t = t_a + t_b$.

IV. RESULTS AND DISCUSSION

In this section we show the results obtained with the experimental procedure described in Sec. III. We measured the macromotion induced by switching on the $\mathbf{B}_m$ field for three values of the initial TOP phase, $\phi_m = 0, \pi/4, \pi/2$. For $\phi_m = 0$ part of the raw data are shown in Fig. 5. In Fig. 7 we show the measured velocity of the macromotion obtained with the stroboscopic method. The upper and lower panels correspond to $\phi_m = 0$ and $\pi/4$, respectively. The data for $\phi_m = \pi/2$ are not shown but are similar to those for $\phi = 0$ and with the roles of x and y interchanged.

The solid lines in the left panels of Fig. 7 are obtained by fitting Eqs. (17) and (18) to the full data including micromotion and provide the input for calculating the amplitudes. Using the known TOP frequency $\omega/2\pi = 4$ kHz and flight time $\Delta t_{\mathrm{TOF}} = 23$ ms, the fit yields for the velocity amplitudes, phases, and frequency $v_0 = 7.6(2)$ mm/s, $V_{0,x} = 0.7(2)$ mm/s, $V_{0,y} = 5.6(2)$ mm/s, $\phi = 1.00(1)\pi$, $\varphi_x = 0.5(2)\pi$, $\varphi_y = 0.05(2)\pi$, and $\Omega/2\pi = 394(4)$ Hz. The corresponding in-trap amplitudes are $\rho_0 \equiv v_0/\omega = 0.30(1)$ μm, $X_0 \equiv V_{0,x}/\Omega = 0.28(7)$ μm, and $Y_0 \equiv V_{0,y}/\Omega = 2.3(1)$ μm.

The right panels in Fig. 7 are parametric plots of the trajectories obtained by reconstructing the motion in the trap from the velocity fits already described. The trajectories provide a useful way to see the effect of the initial phase of the applied $\mathbf{B}_m$ field, and in addition the upper panel can be directly compared with the theoretical prediction shown in Fig. 2. As expected, the orientation of the major axis of the macromotion is dependent on the initial phase ϕ_m of the $\mathbf{B}_m$ field. The small tilt θ away from the direction perpendicular to $\hat{\boldsymbol{\rho}}_m$ is clearly visible and consistent with the calculations for a finite switch-on time and the presence of gravity. The value

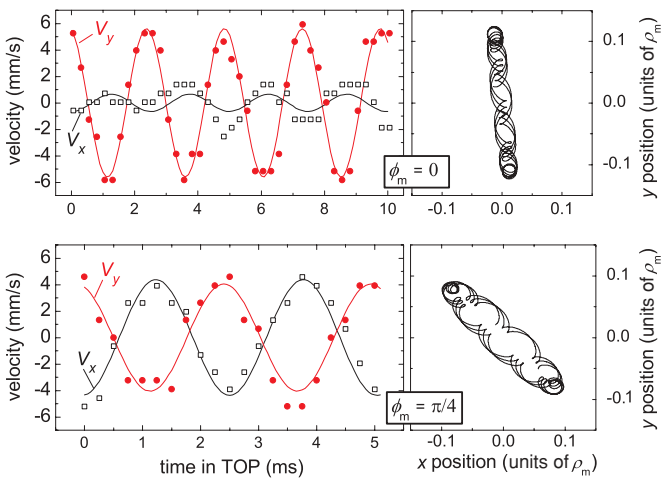

FIG. 7. (Color online) Left panels show the macromotion velocities (taken with the stroboscopic method) of the cloud centroid x (black) and y (red) versus time for $\phi_m = 0$ and $\pi/4$. Solid curves are fits of Eqs. (17) and (18) to the data. Right panels represent the reconstructed trajectories in parametric form (in units of the TOP radius $\rho_m = 19.5$ μm). The difference in aspect ratio is caused by the gravity shift.

TABLE II. Experimental results (expt.) for macromotion induced by the switch-on of the TOP field for $\phi_m = 0, \pi/4$. The data are compared with the results of the numerical calculation of Sec. II C (num). In all cases the tilt angle has be calculated with the aid of Eq. (15).

	ϕ_m	θ/π	φ_x/π	φ_y/π	X_0/ρ_0	Y_0/ρ_0
expt.	0	0.04(2)	0.5(2)	0.05(2)	0.9(2)	7.7(3)
num	0	0.016	0.20	0.06	0.82	6.5
expt.	$\pi/4$	0.04(2)	0.49(2)	0.12(2)	6.6(4)	5.2(3)
num	$\pi/4$	0.013	0.47	0.04	4.95	4.55

obtained for ρ_0 is slightly smaller than the value calculated with Eq. (10), but in view of experimental uncertainties certainly consistent with the value of α. The results for φ_x/π, φ_y/π, X_0/ρ_0,Y_0/ρ_0, and the tilt angle θ obtained for $\phi_m = 0$ and $\pi/4$ are given in Table II. For comparison, the numerical results are also included.

We now turn to the results of a quenching experiment. The time $t_a \simeq 3.83$ ms and magnitude $\Delta\phi_m = -0.22\pi$ of the phase jump have been chosen to meet the conditions necessary to quench the macromotion as introduced in Sec. III B and illustrated in Fig. 6. In Fig. 8 we show velocity data taken with the stroboscopic method. For $t < 3.83$ ms the data coincide with those shown in the upper panel of Fig. 7, but the solid lines are not a fit, representing the macromotion velocity predicted by the numerical calculation on the basis of the experimental parameters. These velocity curves correspond to the macromotion part of the position plot [Fig. 4(b)] and have no adjustable parameters. Both experiment and theory show pronounced reduction in the amplitude of the macromotion. Although the phases of the quenched motion cannot be determined convincingly with our signal-to-noise ratio, the agreement between theory and experiment is satisfactory.

In general a jump in the micromotion phase produces an abrupt change in macromotion phase and amplitude. For the case illustrated in Fig. 8 we obtain a reduction of more than a factor of 5 in the amplitude of oscillation in the y direction at the expense of only a slight increase of the amplitude in the x

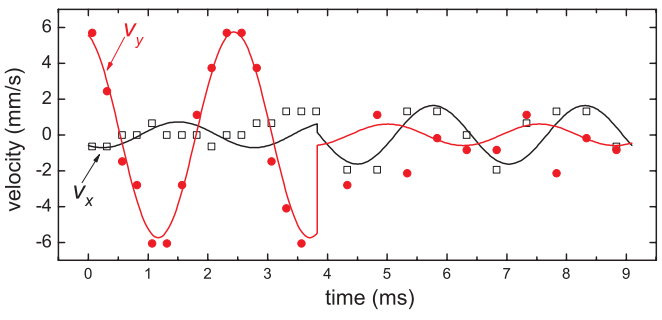

FIG. 8. (Color online) Measured and calculated velocity of the macromotion before and after a phase jump of $\Delta\phi_m = -0.22\pi$ at $t_a = 3.83$ ms for initial phase $\phi_m = 0$. The open black squares (solid red circles) correspond to the measured V_x (V_y) velocity component (for $t_a < 3.83$ ms the data coincide with those of Fig. 7). Each point represents a single measurement. The solid lines correspond to the numerical model without any adjustable parameter as described in the text.

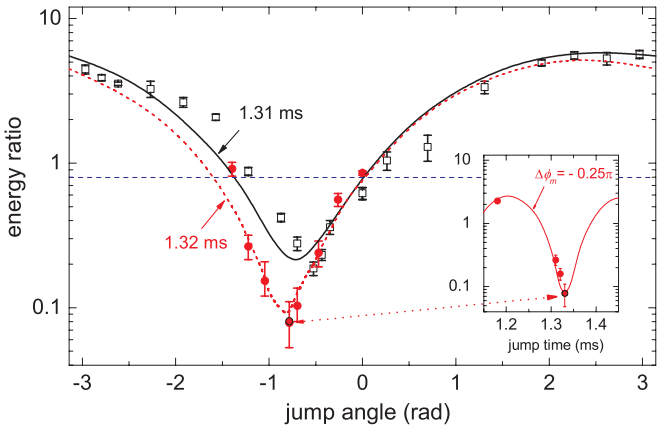

FIG. 9. (Color online) Ratio of macromotion energy over micromotion energy following a phase jump plotted against $\Delta\phi_m$ at 1.32 ms (open black squares) and 1.33 ms (red circles). Each data point is obtained from fits as described in the text. The horizontal blue dashed line shows the initial value of the energy before the phase jump. The solid black lines and dotted red are the numerical calculation for 1.31 and 1.32 ms, respectively. The inset shows the dependence on jump time for fixed value of $\Delta\phi_m$.

direction. As a result the macromotion is reduced to the size of the micromotion. The energy associated with the macromotion is consequently reduced by a factor of about 15, reducing it to a small fraction of the micromotion energy. This demonstrates that the initial sloshing motion of the cloud can be efficiently quenched by applying an appropriate phase-jump angle. As pointed out at the end of Sec. II D, we expect that it should be possible to suppress the macromotion almost completely by adjusting the micromotion frequency such that $t_3 = t_a$.

Even a small variation in the phase-jump magnitude or its timing can result in a substantial difference in quenching efficiency. This is illustrated in Fig. 9, where we plot the ratio of macro- and micromotion energy,

$$\frac{E_{\text{macro}}}{E_{\text{micro}}} = \frac{V_{0,x}^2 + V_{0,y}^2}{v_0^2}, \tag{19}$$

as the phase jump is varied in steps of 10 degrees, for $t_a = 1.32$ and 1.33 ms, where the position and velocity criteria are well satisfied. For most phase jumps $\Delta\phi_m$ the result is an *increase* in energy. The drawn lines are the predictions from the numerical model for the same conditions at $t_a = 1.31$ and 1.32 ms. The plot for $t_a = 1.32$ ms shows a deeper reduction than that for $t_a = 1.31$ ms, as well as a shifted optimal $\Delta\phi_m$. The common shift of ~0.01 ms between the data and the numerical results remains unexplained.

V. SUMMARY AND CONCLUSION

We have shown that a cold atomic cloud initially at rest at the minimum of the effective potential of a TOP trap acquires a macroscopic sloshing motion, in addition to near-circular micromotion, when the TOP is suddenly switched on. The energy associated with this macromotion is of the same order as the energy of the micromotion, and the amplitude of the former is larger than that of the latter by a factor $\sim \omega/\Omega$. We have theoretically described the phenomenon, and the predictions compare well with our experimental results.

As the micromotion is shared in common mode by all trapped atoms, the associated energy does not affect the thermodynamics of the cloud in any way. In contrast, the macromotion energy is generally unwanted and potentially harmful. Fortunately, as we have shown, it is possible to quench this macromotion almost completely and instantly by applying a suitable and properly timed phase jump to the rotating magnetic field that defines the TOP. We have shown theoretically that this procedure works, even for the 2D case of the TOP, which is an extension of previous theory describing similar phenomena in 1D [6,7]. We have presented a framework that allows a deterministic procedure for choosing the optimal parameters for the phase jump. Our experiments corroborate the theoretical model for the TOP in a quantitative manner.

The macromotion induced by the switch-on and the subsequent possibility of altering this motion by phase jumps have several consequences, some of which we now briefly mention. For example, the sloshing motion may affect the time of flight imaging once the fields have been switched off. When comparing TOF images for different holding times it is in general not sufficient to synchronize the release time to the micromotion period. The position after TOF can be easily polluted by the nonzero macromotion, which evolves asynchronously with the micromotion. The time scales in this experiment are on the order of a few macromotion periods. The physics of interest of the cloud is usually seen on much longer time scales of hundreds of such periods. On these longer time scales, the presence of even small anharmonicities can lead to the conversion of macromotion energy into heat. The macromotion can be of an order of the chemical potential, which can have consequences for the stability of the condensate.

The possibility to excite or quench macromotion by phase jumps of the rotating field is a valuable feature of the TOP trap that has received little attention in the literature. Our work shows that this feature is well understood and can be applied in a well-controlled manner. We have primarily focused on quenching with a single phase jump. However, the reverse effect in which the macromotion is excited may prove equally useful in some experiments. Also the consequences for multiple phase-jump applications deserve attention in this respect. We established numerically that it should be possible to excite or deexcite large macromotion with a series of π phase jumps at intervals of the macromotion half period. At each of these phase jumps, either component of the macromotion velocity can be increased or decreased by $\sim 2v_0$. Because this is outside the primary focus of this paper, we do not further elaborate on this interesting topic.

ACKNOWLEDGMENTS

We would like to thank T. G. Tiecke for fruitful discussions and sharing his trap calculation program. JTMW thanks J. Dalibard for a valuable discussion. This work is part of the research program on Quantum Gases of the Stichting voor Fundamenteel Onderzoek der Materie (FOM), which is financially supported by the Nederlandse Organisatie voor Wetenschappelijk Onderzoek (NWO).

APPENDIX: ANALYTIC MODEL

For arbitrary ϕ_m the position $\boldsymbol{\rho}' = \{x', y'\}$ with respect to a coordinate system rotated over an angle ϕ_m is

$$x'(t) = -\rho_0 \cos \omega t + X_0' \cos(\Omega t + \varphi_x'), \tag{A1}$$

$$y'(t) = -\rho_0 \sin \omega t + Y_0' \sin(\Omega t + \varphi_y'), \tag{A2}$$

where X_0', Y_0' are the amplitudes and φ_x', φ_y' the phases with respect to the rotated axes. Taking the time derivative and using the initial conditions $\boldsymbol{\rho}', \dot{\boldsymbol{\rho}}' = 0$ at $t = 0$, yields $\varphi_x' = \varphi_y' = 0$, $X_0' = \rho_0$, $Y_0' = (\omega/\Omega)\rho_0$. This corresponds to an ellipse with its major axis oriented perpendicular to the instantaneous direction $\hat{\boldsymbol{\rho}}_m' \equiv \hat{\boldsymbol{\rho}}_m$ of the $\mathbf{B}_m$ field at $t = 0$.

For exponential switch-on of the $\mathbf{B}_m$ field with $1/e$ time τ_0, we have for the acceleration in the "primed" coordinate system

$$\ddot{x}'(t) = \omega^2[1 - \exp(-t/\tau_0)]\rho_0 \cos \omega t - \Omega^2 X_0' \cos(\Omega t + \varphi_x'), \tag{A3}$$

$$\ddot{y}'(t) = \omega^2[1 - \exp(-t/\tau_0)]\rho_0 \sin \omega t - \Omega^2 Y_0' \sin(\Omega t + \varphi_y'), \tag{A4}$$

where, during switch-on, X_0', Y_0', φ_x', φ_y', and Ω are functions of time. Since $\Omega \ll \omega$, we may approximate, for $\omega t \ll 1$,

$$\ddot{x}'(t) \simeq \omega^2[1 - \exp(-t/\tau_0)]\rho_0 \cos \omega t \gg \ddot{y}'(t). \tag{A5}$$

This shows that the switch-on profile mainly affects the acceleration in the x' direction because this is the initial direction of acceleration. By the time $\sin \omega t$ is sufficiently large to make $\ddot{y}'$ nonnegligible, the switch-on transient is already finished. For $\omega t \ll 1$, the velocity in the x' direction is given by $\dot{x}'(t) \simeq \omega^2[t - \tau + \tau \exp(-t/\tau)]\rho_0$. This expression suggests approximating the switch-on profile by a step function at $t = \tau_0 \simeq \tau$ and treating X_0', Y_0', φ_x', φ_y' as constants for $t \geqslant \tau_0$. This "delayed sudden-step approximation" is equivalent to imposing the boundary conditions $\boldsymbol{\rho}'$, $\dot{\boldsymbol{\rho}}' = 0$ at $t = \tau_0$. In this approximation we obtain for the phases and amplitudes $\varphi_x' = \tan^{-1}[\omega^2\tau_0/\Omega], \varphi_y' = 0, X_0' = \rho_0(1 + \omega^4\tau_0^2/\Omega^2)^{1/2}$, and $Y_0' = (\omega/\Omega)\rho_0$ for $t \geqslant \tau_0$. The phase development $\omega\tau_0$ due to rotation of the $\mathbf{B}_m$ field during switch-on will appear as a rotation of the major and minor axes of the macromotion with respect to the primed coordinate system defined by $t = 0$. The optimal value for τ_0 can be determined by comparing the predictions of the analytical model with the results of a numerical calculation (see Sec. II C).

In the presence of gravity, this analysis remains valid as long as the radial frequency Ω does not change substantially during switch-on of the $\mathbf{B}_m$ field; in principle Ω can be kept constant by simultaneously switching B_0 and B_m in such a way that the quantity $\bar{B}_0/(1 + \frac{1}{2}B_m^2/\bar{B}_0^2)$ equals the value of B_0 before the $\mathbf{B}_m$ field was switched on. In case of a small and fast change in Ω our model can be adapted by changing the initial conditions to $\boldsymbol{\rho} - \{0, \delta y\}, \dot{\boldsymbol{\rho}} = 0$ at $t = \tau_0$, where $\delta y = \Delta y_{\mathrm{TOP}} - \Delta y_{\mathrm{IP}}$ is the difference in gravitational sag. Using the adapted boundary conditions we obtain in the limits $(g\alpha/\bar{B}_0)^{1/2} \ll \Omega \ll \omega$ and $\omega\tau_0 \ll 1$ for the amplitudes and phases of the macromotion

$$X_0 = \rho_0[1 + (\omega^2/\Omega^2 - 1)\sin^2(\omega\tau_0 + \phi_m)]^{1/2}, \tag{A6}$$

$$Y_0 = \rho_0\big[1 + (\omega^2/\Omega^2 - 1)\cos^2(\omega\tau_0 + \phi_m) + \delta y^2/\rho_0^2 + 2(\delta y/\rho_0)\sin(\omega\tau_0 + \phi_m)\big]^{1/2}, \tag{A7}$$

$$\varphi_x = -\Omega\tau_0 + \tan^{-1}\left[(\omega/\Omega)\tan(\omega\tau_0 + \phi_m)\right] + n\pi, \quad \text{(A8)}$$

$$\varphi_y = -\Omega\tau_0 + \tan^{-1}\{(\Omega/\omega)[\tan(\omega\tau_0 + \phi_m) + (\delta y/\rho_0)/\cos(\omega\tau_0 + \phi_m)]\} + n\pi, \quad \text{(A9)}$$

where $n = 0$ for $|\omega\tau_0 + \phi_m| \leqslant \pi/2$, $n = 1$ for $|\omega\tau_0 + \phi_m| > \pi/2$. For $\phi_m = 0$, these equations coincide with the equations for X_0', Y_0', φ_x', and φ_y' in the primed coordinate system. Analyzing the limit $\omega\tau_0 \to 0$ for the case $\delta y \simeq \rho_0$ (typical for our experimental conditions), we find $X_0 \simeq \rho_0$ and $Y_0 \simeq (\omega/\Omega)\rho_0$ for $\phi_m = 0$ and $X_0 \simeq (\omega/\Omega)\rho_0$ and $Y_0 \simeq 2\rho_0$ for $\phi_m = \pi/2$. Thus, we deduce that gravity can have a substantial influence on the amplitude of the macromotion along its minor axis but not on the amplitude along the major axis. For known values of X_0, Y_0, φ_x, and φ_y the angle of rotation ϑ to align the coordinate system along the major and minor axis is given by Eq. (15). For $\Omega\tau_0 \ll \omega\tau_0 \ll 1$ and in the absence of gravity ($\delta y = 0$) the delayed sudden step gives rise to a small rotation $\Delta\varphi \simeq \omega\tau_0$, independent of ϕ_m. For $\delta y \simeq \rho_0$ gravity gives rise to an additional contribution to this rotation, which is minimal for $\phi_m = \pi/2$, where the macromotion is launched perpendicular to the gravity direction and Eq. (15) can be approximated by $\varphi \simeq \omega\tau_0[1 + (1 + \delta y/\rho_0)(\Omega/\omega)^2]$. The contribution is maximal for $\phi_m = 0$, where Eq. (15) can be approximated by $\varphi \simeq \omega\tau_0 - (\Omega/\omega)^2(\delta y/\rho_0)^2(1 + \omega\tau_0)$.

Insight into the dependence of X_0 and Y_0 on the settling behavior of B_0 can be obtained from Eq. (A5), which shows that the initial acceleration and, hence, the launch speed scales with the initial value of ρ_0. Therefore, most of the settling behavior is captured by using the *initial* value of ρ_0 in Eqs. (A6) and (A7). The 5% change in Ω requires a further refinement of the model. This cannot be implemented without sacrificing the simplicity of the model and is not pursued here.

[1] W. Petrich, M. H. Anderson, J. R. Ensher, and E. A. Cornell, Phys. Rev. Lett. **74**, 3352 (1995).

[2] M. H. Anderson, J. R. Ensher, M. R. Matthews, C. E. Wieman, and E. A. Cornell, Science **269**, 198 (1995).

[3] A. L. Migdall, J. V. Prodan, W. D. Phillips, T. H. Bergeman, and H. J. Metcalf, Phys. Rev. Lett. **54**, 2596 (1985).

[4] T. Bergeman, G. Erez, and H. J. Metcalf, Phys. Rev. A **35**, 1535 (1987).

[5] D. S. Hall, J. R. Ensher, D. S. Jin, M. R. Matthews, C. E. Wieman, and E. A. Cornell, Proc. SPIE **3270**, 98 (1998).

[6] A. Ridinger and N. Davidson, Phys. Rev. A **76**, 013421 (2007).

[7] A. Ridinger and C. Weiss, Phys. Rev. A **79**, 013414 (2009).

[8] M. Edwards, R. J. Dodd, C. W. Clark, P. A. Ruprecht, and K. Burnett, Phys. Rev. A **53**, 1950(R) (1996).

[9] V. I. Yukalov, Phys. Rev. A **56**, 5004 (1997).

[10] V. G. Minogin, J. A. Richmond, and G. I. Opat, Phys. Rev. A **58**, 3138 (1998).

[11] A. B. Kuklov, N. Chencinski, A. M. Levine, W. M. Schreiber, and J. L. Birman, Phys. Rev. A **55**, 488 (1997).

[12] R. Franzosi, B. Zambon, and E. Arimondo, Phys. Rev. A **70**, 053603 (2004).

[13] K. J. Challis, R. J. Ballagh, and C. W. Gardiner, Phys. Rev. A **70**, 053605 (2004).

[14] D. J. Han, R. H. Wynar, Ph. Courteille, and D. J. Heinzen, Phys. Rev. A **57**, 4114(R) (1998).

[15] M. Kozuma, L. Deng, E. W. Hagley, J. Wen, R. Lutwak, K. Helmerson, S. L. Rolston, and W. D. Phillips, Phys. Rev. Lett. **82**, 871 (1999).

[16] B. P. Anderson and M. A. Kasevich, Phys. Rev. A **59**, 938(R) (1999).

[17] J. H. Müller, O. Morsch, D. Ciampini, M. Anderlini, R. Mannella, and E. Arimondo, Phys. Rev. Lett. **85**, 4454 (2000).

[18] D. R. Scherer, C. N. Weiler, T. W. Neely, and B. P. Anderson, Phys. Rev. Lett. **98**, 110402 (2007).

[19] O. M. Maragò, S. A. Hopkins, J. Arlt, E. Hodby, G. Hechenblaikner, and C. J. Foot, Phys. Rev. Lett. **84**, 2056 (2000).

[20] S. R. Muniz, D. S. Naik, and C. Raman, Phys. Rev. A **73**, 041605(R) (2006).

[21] T. G. Tiecke, M. Kemmann, C. Buggle, I. Schvarchuck, W. von Klitzing, and J. T. M. Walraven, J. Opt. B: Quantum Semiclass. Opt. **5**, S119 (2003).

[22] N. R. Thomas, N. Kjærgaard, P. S. Julienne, and A. C. Wilson, Phys. Rev. Lett. **93**, 173201 (2004).

[23] C. Buggle, J. Leonard, W. von Klitzing, and J. T. M. Walraven, Phys. Rev. Lett. **93**, 173202 (2004).

[24] O. J. Luiten, Ph.D. thesis, University of Amsterdam, 1993.

[25] E. L. Surkov, J. T. M. Walraven, and G. V. Shlyapnikov, Phys. Rev. A **49**, 4778 (1994).

[26] We verified that the approximation $\phi = \phi_m + \pi$ holds to within one degree for conditions relevant for our analysis.

[27] K. Dieckmann, Ph.D. thesis, University of Amsterdam, 2001.

[28] C. Buggle, Ph.D. thesis, University of Amsterdam, 2005.